Strong Metal-support Interaction (SMSI) Modulates d-orbital Centers to Promote Oxygen Reduction Reaction

Zhangmeng Liu[a], Guiting Lin[b], Yayao Li[b], Runchao Zhou[b], Yunzhi Fu*[b]

[a] School of Materials Science and Engineering, Hainan University, Haikou, 570228, P.R. China
E-mail: zliu626@hainanu.edu.cn
[b] School of Chemistry and Chemical Engineering, Hainan University, Haikou 570228, P.R. China
E-mail: yzhfu@hainanu.edu.cn

Experimental Procedures.....3

Materials.....3

Preparation of CN and ACN 3

Characterization.....4

Density functional theory (DFT) calculations.....5

Photo-electrochemical measurements.....6

Photocatalytic activity test.....6

Results.....6

Figure S1.....10

Figure S2.....11

Figure S3.....11

Figure S4.....12

Figure S5.....13

Figure S6.....14

Figure S7.....15

Figure S8.....16

Figure S9.....16

Figure S10.....17

References.....18

Experimental section

Materials

Urea (CH_4N_2O), melamine ($C_3H_6N_6$), Hydrochloric acid (HCl), hydrogen peroxide (H_2O_2), Methanol, L-Histidine, Ammonium oxalate, benzoquinone, was obtained from Mclean Chemistry Co., Ltd., sodium hydroxide (NaOH) and Isopropanol (C_3H_8O analytical reagent) were purchased from Xilong Science Co., Ltd., sodium sulphate (Na_2SO_4), isopropanol (C_3H_8O, analytical reagent, ≥ 99.7%), and silver nitrate ($AgNO_3$) were purchased from Sinopharm Chemical Reagent Co. Ltd. (Shanghai, China); and 5-dimethyl-1-pyrrole-N-oxide (DMPO, 99.5%), 2,2,6,6-Tetramethylpiperidine-1-oxyl (TEMPO), Nitrotetrazolium Blue chloride (NBT) and 4,4'-Diamino-3,3', 5,5'-tetramethyl biphenyl (TMB, analytical reagent) were obtained from Mclean Chemistry Co., Ltd. All reagents are analytically pure and can be used without further treatment. Deionized water (18.2 MΩ·cm) was used for all preparations.

Preparation of CN and ACN

CN was carried out according to the previous work of our group. Specifically, a certain amount of urea was put into a crucible with a capacity of 50 mg, and a thermal polymerization reaction was carried out in a tube furnace chamber filled with ammonia gas at a heating rate of 5 ℃/min. The temperature was kept at 550 ℃ for two hours, then slowly cooled to room temperature. The resulting powder material was labeled CN.

Preparation of ACN: Ag clusters-CN-based structure (abbreviated as ACN) with intercalated and semi-intercalated structure was synthesized by molecular self-assembly method under argon protection. Specifically, melamine and urea were dissolved and mixed in water, and a small amount of $AgNO_3$ solution was added to stir uniformly. Finally, the chelated precursor was placed in a quartz dish and sealed. ACN structure was obtained by setting the tube furnace at 550℃, heating it for 3h, and slowly cooling it to room temperature.

For comparison, Ag nanoparticle-supported CN structures were synthesized. 100 mg of CN prepared above was ultrasonically dispersed in 100 mL ultrapure water, 1 mM $AgNO_3$ aqueous solution (5, 10, 15, 20, 30, 45 mL) was added to the above solutions respectively, and irradiated under simulated sunlight of 100 mW/m^2 for 15 min. After the $AgNO_3$ solution was completely reduced, the solution was centrifuged, and the precipitate was washed, dried, and collected.

Characterization

The microstructure and morphology of the samples were observed by Talos F200X G2 (SEM) and (TEM). X-ray diffraction (XRD) patterns (Rigaku DX-2700BH), X-ray photoelectron spectroscopy (XPS) spectra were to characterize samples' crystal and molecular constitution. Optical performance was evaluated with a UV-Vis-NIR spectrophotometer ((Shimadzu, UV2450) and steady-state photoluminescence spectrum (PL, FLS 880). The ultraviolet-visible (UV-vis) absorption spectra were recorded from 200 − 800 nm using a UV-Vis-NIR spectrophotometer (Agilent S3 Cary 5000) with $BaSO_4$ reflectance standards. The electron paramagnetic resonance (EPR) spectra were carried out at 110 K using a JEOL JESFA200 EPR spectrometer. For the free radical test, 5,5-dimethyl-1-pyrroline N-oxide (DMPO) were used as a spin-trapping reagent to detect •OH or $•O_2^-$. The EPR spectra were carried out at 300 K using water or methanol mixed with 5,5-dimethyl-1-pyrroline N-oxide (DMPO). A 300 W Xe lamp (λ ≥ 400 nm) was used as the light source. The methanol mixtures were purged with N_2 gas before light irradiation. Samples for X-ray photoelectron spectroscopy (XPS) measurements were collected using an SSI S-Probe XPS spectrometer. AFM images were obtained using an NT-MDT Solver Next atomic force microscope. Atomic Force Microscopy (AFM) images were acquired from a Bruker Dimension Icon using the Peakforce Tapping model, where the catalysts were diluted in ethanol and then dropped onto a mica plate. The LED light model and power is a full white LED lamp with a wavelength range of 400 - 830 nm (220V 13W). XANES and EXAFS spectra of AgK edge at room temperature have been measured using transmission mode at SSRF BL14W1 line station. XPS and UPS data were obtained using a Thermo Fisher ESCALAB Xi+ spectrometer. Nitrogen adsorption-desorption isotherms were

conducted using a Surface Area and Porosity Analyzer (ASAP 2020, Micromeritics) at 77K after degassing the samples at 150 °C for 4h. The steady-state PL emission spectra and time-resolved transient PL decay spectra were measured at room temperature using a PTI QM-4 fluorescence spectrophotometer. Piezo electrochemical measurements were operated in a standard three-electrode system (CHI 660E electrochemical station) under ultrasonic irradiation (generated by an ultrasonic cleaner, KQ-300DE, Kunshan). The three-electrode system was composed of the samples as the working electrode, Ag/AgCl (saturated KCl) as the reference electrode and Pt wire as the counter electrode. 0.1 M Na_2SO_4 solution was used as the electrolyte. Conductive adhesive was used to fix the samples on ITO glass tightly. The stable adsorption energy and free energy of various models are first optimized through Forcite module, and the forcefield is the COMPASS II module. Then, the Dmol3 module is used to search the transition state and calculate the stable adsorption energy, electron localization function (ELF), electron density difference (EDD) and primordial cells' tape constitution were evaluated through the Dmol3 module. The generalized gradient estimation (GGA) of Perdew-Burke-Ernzerhof (BP) operational is invoked for correlation and electron exchange. The level wave base's cutoff power is set to 450 eV, and the mutual space's k point is placed to an exceptional standard. All the structures are completely relaxed, and the force tolerance is 1.0 e^{-5} eV.

Density functional theory (DFT) calculations

The geometries of the different CN materials were reduced to a simple repeating unit. States' density (DOS) and primordial cells' tape constitution were evaluated through the CASTEP module. The generalized gradient estimation (GGA) of Perdew-Burke-Ernzerhof (PBE) operational is invoked for correlation and electron exchange. The level wave base's cutoff power is set to 450.0 eV, and the mutual space's k point is placed to an exceptional standard. The interaction between contiguous pictures in the optimization unit's computation is eradicated at the side of 15 vacuum layers. All the structures are completely relaxed, and the force tolerance is 0.02 eV.

These units and adsorption structures of O_2/H^+ were optimized with dispersion-corrected density functional theory (DFT-D_3) at the PBE$_0$-D_3/def$_2$-SVP [1] + SDD [2] level

using the Gaussian 16 program. Vibrational frequency analyses were carried out for these optimized structures using the same calculation method to obtain zero-point and free energy corrections. Finally, the single point energy was added to the free energy correction calculated before to obtain the Gibbs free energy. [3] The adsorption free energy of the complex was calculated from the formular:

$$G_{(adsorb)} = G_{(A+B)} - G_{(A)} - G_{(B)}$$

where G(A) and G(B) is the Gibbs free energy of isolated molecules, G(A+B) is the total free energy of the complex structure.[4]

Photo-electrochemical measurements

Through CHI 760D electrochemical, the electrochemical impedance and photocurrent reaction of prepared photocatalysts were gauged in a conventional three-electrode system (CH Implements, Inc., China). The three electrodes consisted of catalyst-coated indium-doped can oxide (ITO) glass (2 cm×2 cm) as the functional electrode, Pt wire as the counter electrode, and a strong calomel electrode (SCE) as the mentioned electrode. In the meantime, Na_2SO_4 solution (0.1 M 50 mL) was utilized as an electrolyte solution. The functional electrode was prepared (500 μL) of the prepared dynamic substance on an ITO glass substrate through drop-casting an aliquot. An aliquot was prepared by dispersing the synthesized powdered sample's 1 mg ultrasonically with 5 mL of deionized water and adding 5 μL of Nafion solution (1%) as a binder. The temporary photocurrent (i-t) was deliberately consuming the equivalent 300W Xenon lamp at 0.5 V utilized potentiality. The electrochemical impedance spectroscopy (EIS) research was executed in the frequency scope of 1000 Hz - 8000 Hz with a sinusoidal AC indication of 10 mV.

Photocatalytic H_2O_2 production.

The photosynthesis of H_2O_2 was performed in a multi-channel photochemical reaction system (Beijing Perfectlight, PCX-50C). Specifically, 20 mg catalyst was dispersed into 80 mL deionized water in a quartz glass bottle (maximum diameter, φ60 mm; capacity 100 ml)

with a rubber septum cap sealing the bottle. The catalyst was dispersed under ultrasonication for 15 min and bubbled with O_2 for 30 min. The air experiment was done by bubbling air continuously into the solution for 30 min, and the light was then turned on after 30 min of bubbling. Each sample was continued to be continuously bubbled with a syringe after each sampling, and then the light was turned on for the next cycle of light reaction. The LED lamp (λ ≥ 400 nm) was used to irradiate the photocatalyst suspension from the bottom. The bottle was kept at 25 ± 0.5 °C via cooling water, and then a 1 mL aliquot was collected from the suspension at a given time interval (10 min).

The concentration of H_2O_2 was determined by the enzyme chromogenic method. 2.8756 g of dipotassium hydrogen phosphate ($K_2HPO_4 \cdot 3H_2O$) and 11.935 g of potassium dihydrogen phosphate (KH_2PO_4) were dissolved in 200 mL water to prepare 1M (pH=7) PBS buffer. 100 mg DPD was dissolved in 10 mL 0.05 M H_2SO_4 solution to prepare DPD solution. 10 mg POD was dissolved in 10 mL ultra-pure water to prepare the POD solution. The sample solution diluted by 2.15 mL was mixed with 0.40 mL PBS buffer. Then 50 μL DPD solution and 50 μL POD solution were added successively and stirred for 30 s. The Abs of the mixture at the wavelength from 700 nm to 400 nm was measured by ultraviolet-visible spectrophotometer (UV-Vis) as soon as possible, and the corresponding H_2O_2 concentration was calculated by the standard curve. 2.24 mL deionized water, 0.8 mL PBS buffer, 0.1 mL DPD solution and 0.1 mL POD solution were removed by liquid transfer gun and mixed in 10 mL centrifuge tube to get the mixed solution. The H_2O_2 standard solutions (10, 50, 100, 200 and 500 μM) with 2 mL configuration were added to the mixed solution. After the solution was mixed slowly for 30 seconds, it was transferred to a quartz colorimetric plate, and then the absorbance values of different concentrations of H_2O_2 standard solution at 551 nm wavelength were determined by UV-Vis. Finally, the standard curve is drawn by linear quasi-merging with the concentration of H_2O_2 standard solution (C) as Abscissa and absorbance value (A) as ordinate.

Rotating ring disk electrode (RRDE) electrode Measurements. The electron transfer number was obtained using an electrochemical workstation (CHI660E) by a three-electrode cell with Rotating ring Disc Electrode (RRDE) as working electrode, graphite rod

as counter electrode, calomel electrode as reference electrode and 0.1 M Na_2SO_4 as electrolyte. Generally, each of sample and carbon powder (6 mg each) were dispersed in isopropanol (600 μL) with 30 min sonication, followed by the addition of Naphthol reagent (10 μL) to the mixture and sonication for 15 min to obtain the ink. The ink (6 μL) was then dropped onto the glass carbon disc of the RRDE. The disk potential and ringing potential were set to open circuit potential and 1.2 V vs. SCE, respectively

The electron transfer number is acquired via the following equation (1):

$$n=4I_d/(I_d+I_r/N) \quad (1)$$

Here, n is the number of electron transfers, N is the collection efficiency of the Pt ring, while I_d and I_r indicate the disc and ring currents, respectively.

H_2O_2 decomposition study. The decomposition of H_2O_2 was carried out by mixing the catalyst (20 mg) with H_2O_2 (1 mM) aqueous solution (30 mL) and bubbling with N_2 for 30 min. The catalyst was sonically dispersed for 15 minutes and bubbled by N_2 for 30 min. The LED lamp (λ ≥ 400 nm) was used to irradiate the photocatalyst suspension from the bottom. The bottle was kept at 15 ± 0.5 °C via cooling water and then a 2 mL aliquot was collected from the suspension at a given time interval (30 min), filtrated by a syringe filter (0.22 μm) to remove the photocatalyst. Then, the amount of H_2O_2 produced was determined by the iodometric method.

Photocatalytic evolution of $\bullet O_2^-$: The concentration of $\bullet O_2^-$ was measured by detecting the decay of NBT (nitroblue tetrazolium) using UV-vis spectroscopy. 2.5 mL of liquid was filtrated with a 0.22 μm filter to remove the photocatalysts. The photocatalytic generation of $\cdot O_2^-$ was determined by the degradation of NBT, which was detected by the absorbance change at the wavelength of 259 nm. The mole ratio of generated $\bullet O_2^-$ and reacted NBT was 4:1.

Molecular Oxygen Activation Measurements: 50 μL of aqueous suspension of the sample (10 g L^{-1}) and 20 μL of 3,3',5,5'-tetramethylbenzidine (TMB) (50 mM

aqueous solution) were mixed with 2 mL of HAc/NaAc buffer solution. A 300 W xenon lamp (PLS-SXE300/300UV, Trusttech Co., Ltd., Beijing) equipped with a 420 nm cut-off filter was used as the light source. TMB oxidation were evaluated by UV-Vis measurements (the absorbance around 370 nm) at different time intervals. To identify the type of active oxygen species, scavenging experiments were conducted as the above procedure with different amounts of scavengers (mannitol, 50 mM, 100 μL; carotene, 2 mg; catalase, 4000 units/mL, 100 μL; SOD, 4000 units/mL, 100 μL).

Determination of apparent quantum yield. The photocatalytic reaction was conducted on an autoclave with a quartz window in which deionized water (30 mL) and photocatalyst (20 mg) were added, sonicated and bubbled O_2 for 30 min. A 300 W Xenon lamp was used to irradiate the reactor for 1 hour under magnetic stirring with the incident light using band-pass filters at 350 ± 5 nm, 365 ± 5 nm, 380 ± 5 nm, 420 ± 5, 450 ± 5 nm and 500 ± 5 nm, respectively. Illumination intensity was confirmed by a light power meter with an irradiated area of 4.0 cm^2. The apparent quantum yield (AQY) is available from the following equation (2).

$$\text{AQY (\%)} = \frac{H2O2_{generated\,(mol)} \times 2}{N} \times 100\,\% \qquad (2)$$

SCC Efficiency measurements: The solar-to-chemical energy conversion (SCC) efficiency was determined by using an AM 1.5G solar simulator as the light source (100 mW cm^{-2}). Catalysts (40 mg) and water (30 mL) were put in a sealed device mainly composed of a quartz tube. During the photocatalytic tests, O_2 was continually bubbled into the bottle. The SCC efficiency was calculated via the following equation (3):

$$\text{SCC} = \frac{\Delta G_{H2O2} \times n_{H2O2}}{I \times S \times T} \times 100\% = \frac{117 \times 10^3 \times 125 \times 10^{-6}}{100 \times 1 \times 10^{-3} \times 3600} \times 100\% = 1.06\,\% \qquad (3)$$

Where ΔG = 117 kJ mol^{-1}, the irradiated sample areas are 4.0 cm^2 during 0.5 h of illumination. During the photocatalytic reaction, 125.14 μmol H_2O_2 was generated during 1 h.

Results and discussion

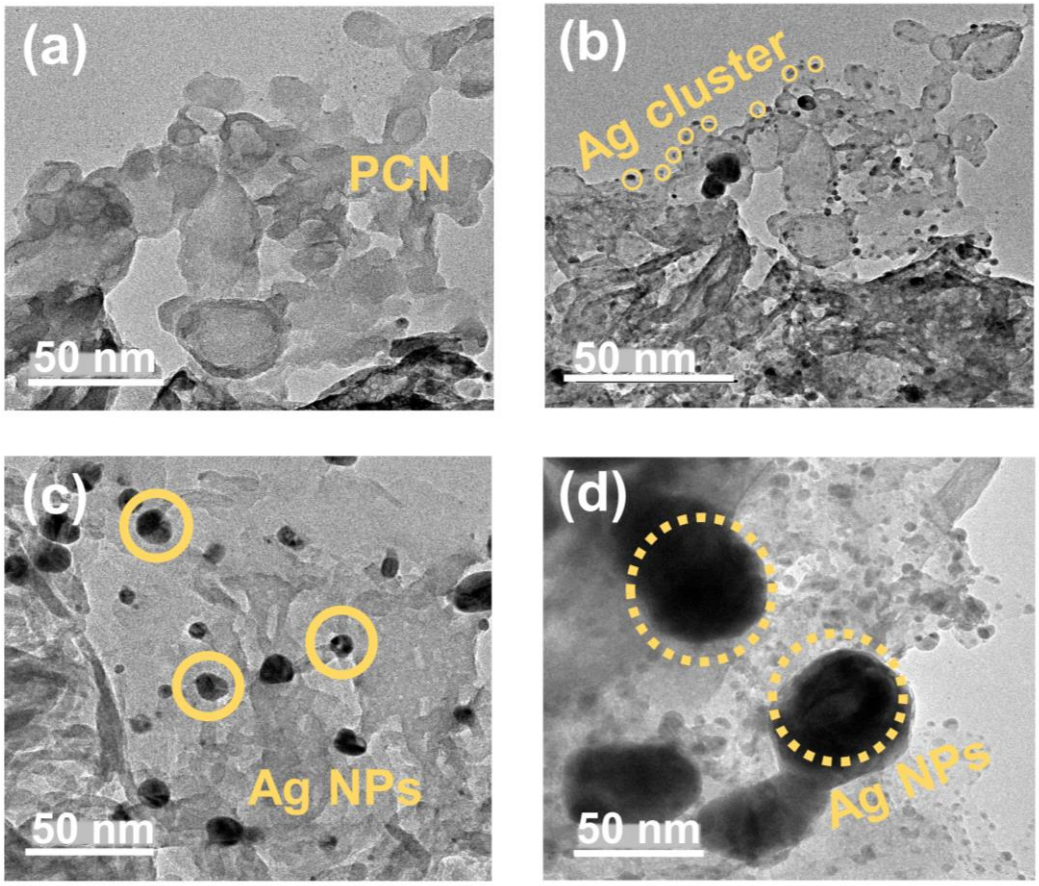

Figure S1 (a) SEM for CN; **(b)** SEM for ACN; **(c)(d)** SEM for Ag NPs@CN

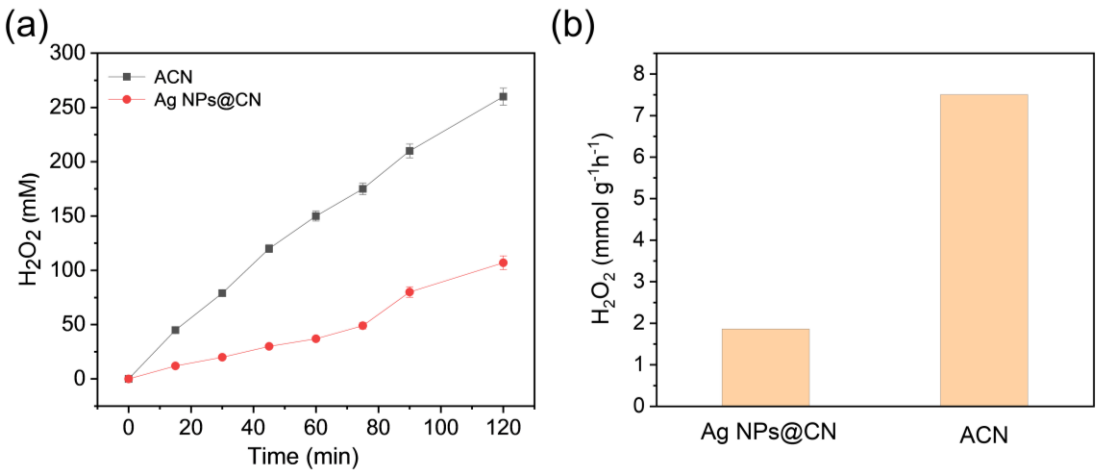

Figure **S2**. (a) Hydrogen peroxide yield curves under different conditions for **a-b** ACN and Ag NPs**@**CN (catalyst: 0.2 g/L; Xe Light: 100 mW/cm^2)

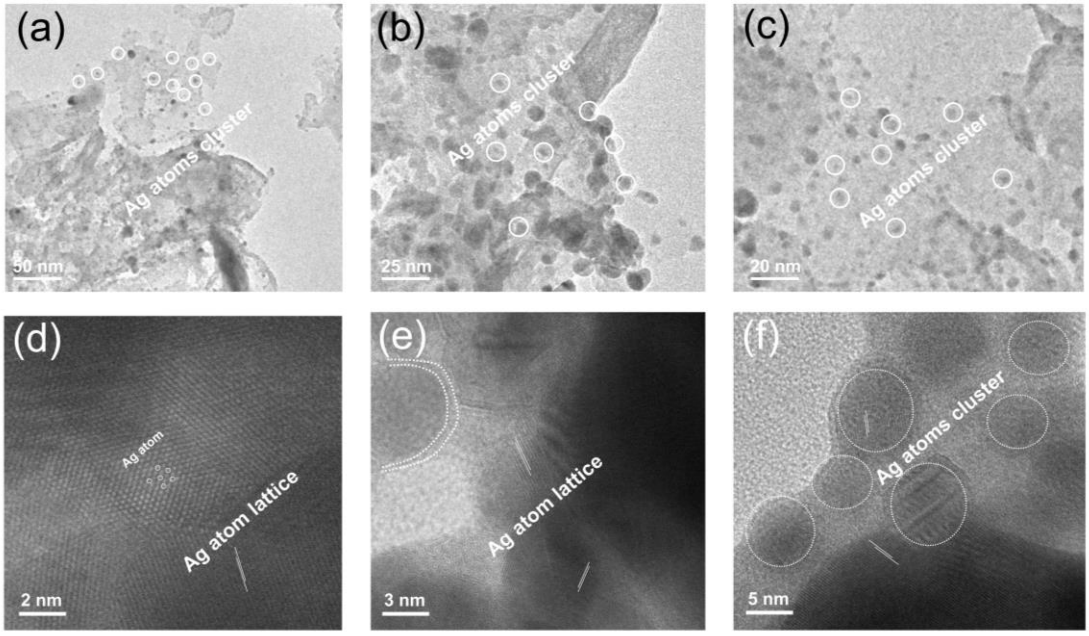

Figure **S3**. (a) – (f) High-resolution dark-field microscopy images of ACN at different sizes

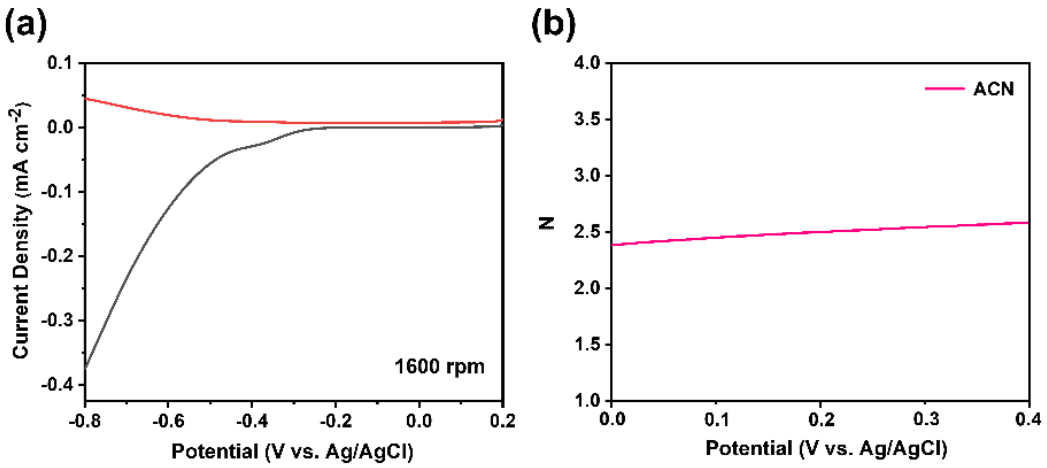

Figure S4 (a) The RRDE polarization curve over ACN-coated electrodes at room temperature at 1600 rpm rotation rates (ω = 1600 rpm). The ring current (top) and disc current (bottom). **(b)** the corresponding number of electro-transfer as a function of the applied potential. The electrochemical measurements were performed in O_2 saturation (0.1 M Na_2SO_4) with a 10 mV s^{-1} scan rate at 1600 rpm.

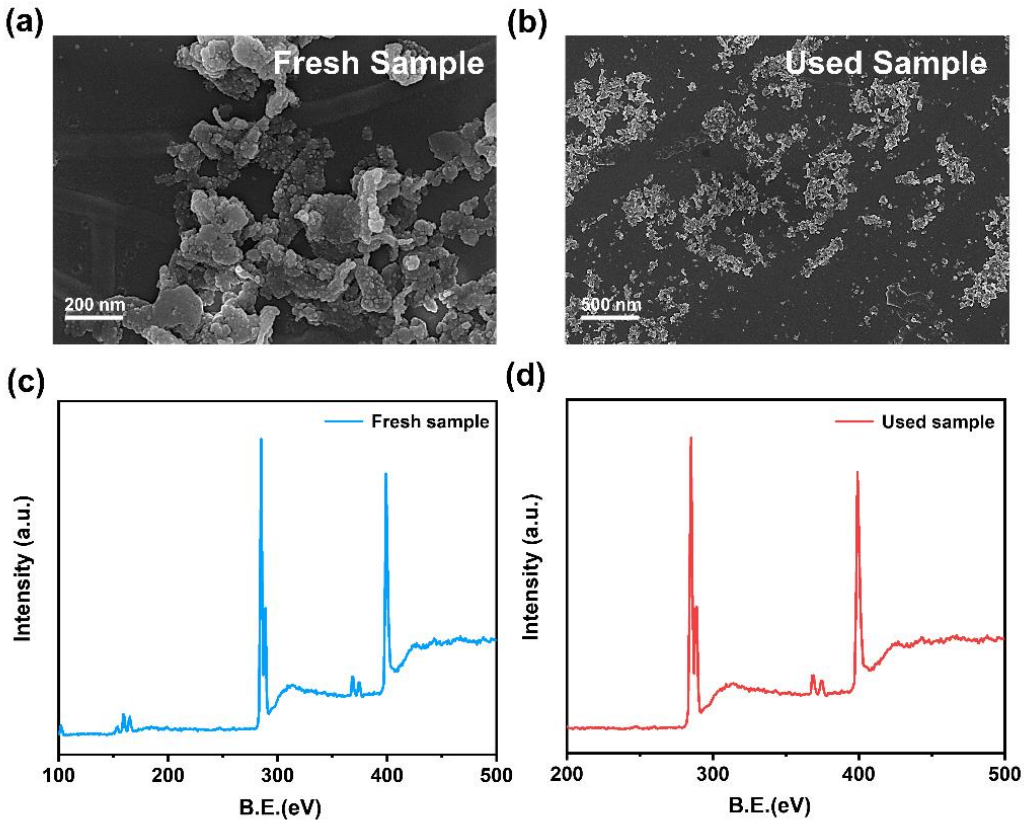

Figure S5 Comparison of morphology, structure and surface properties before and after ACN reaction

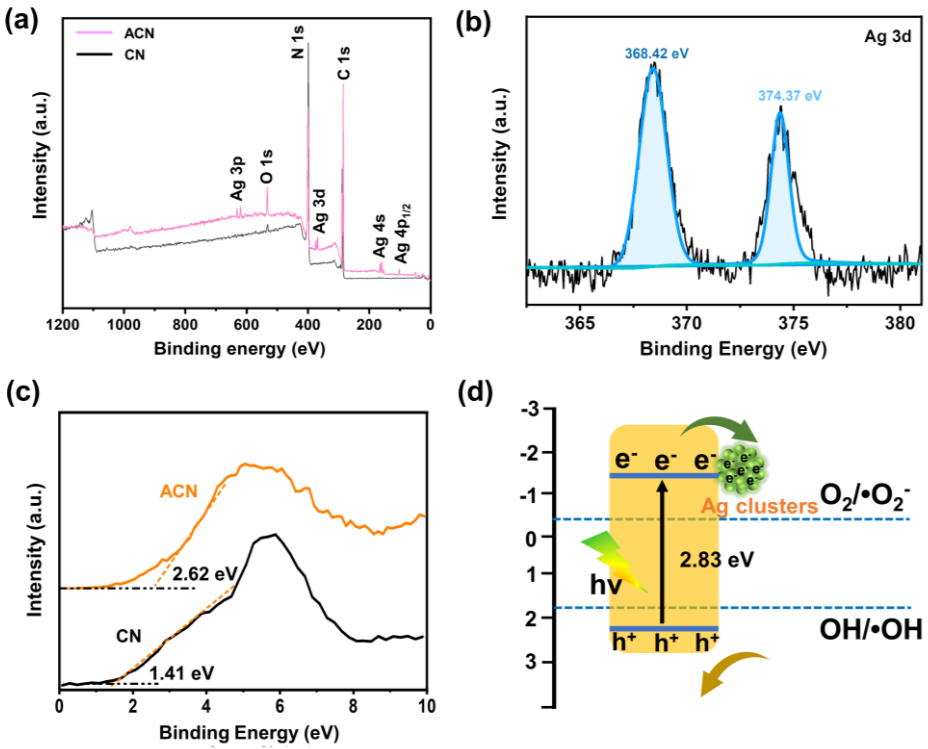

Figure S6 a Survey spectrum of CN and ACN; **b** Ag 3d spectrum of ACN; **c** VB-XPS of samples; **d** Redox potential and energy band position diagram

Most of the valence charge electrons and conduction band electrons of semiconductors are distributed near the band gap, so when the photon energy approaches the band gap width, a large number of electrons can transition by absorbing the photon energy, and the absorption coefficient will increase with the increase of the number of photons. For semiconductor materials, there is the following relationship between the optical bandgap and the absorption coefficient:

$$(\alpha h\nu)^{1/n} = B(h\nu - E_g) \quad (1)$$

Where α is the absorption coefficient, *hv* is the photon energy, h is the Planck constant ($h \approx 4.13567 \times 10^{-15}$ eV • s), v is the incident ray frequency ($v = c/\lambda$, where c is the speed of light, $c \approx 3 \times 10^{8}$ m/s; λ is the wavelength of the incident ray), B is the proportionality constant, and E_g is the band gap width of the

semiconductor material.

The value of n depends on the type of semiconductor material. When the semiconductor material has a direct bandgap, n = 1/2; when the semiconductor material has an indirect bandgap, n = 2.

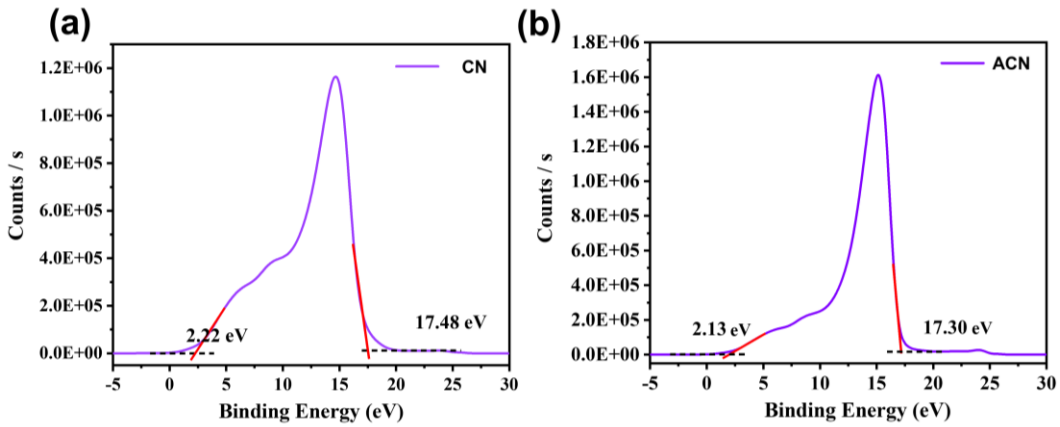

Figure S7. UPS spectrum of samples

Through the conversion method of the valence band value in the reference literature[5], UPS was used to determine the ionization potential, which is equivalent to the valence band energy (E_{VB}). According to the linear intersection method, the E_{VB} of ACN was calculated to be -6.05 eV (vs. vacuum) from hv + E_{Fermi} - E_{Cutoff} (hv of 21.22 eV: the excitation energy of the He I Source Gun). Then the E_{VB} of ACN, vs. RHE, was converted to be 1.61 eV, based on the relationship between the vacuum energy (E_{vacuum}) and the RHE potential (E_{RHE}), E_{vacuum} = -E_{RHE} - 4.44 eV. Knowing the VB maximum difference between ACN and CN, determined from VB XPS spectra, we can get E_{VB} of CN and ACN, vs. RHE. Combined with the bandgap values calculated from UV-vis diffuse reflectance spectra, the band positions of ACN, and CN could be then obtained.

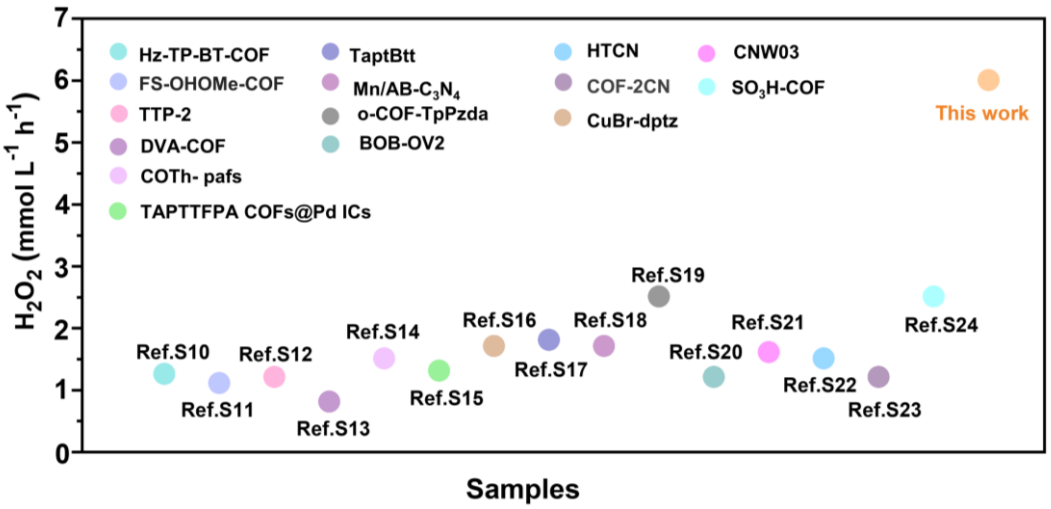

Figure S8 Comparison of H_2O_2 production efficiency between ACN and other covalent polymer catalysts (Corresponding literature: [6])

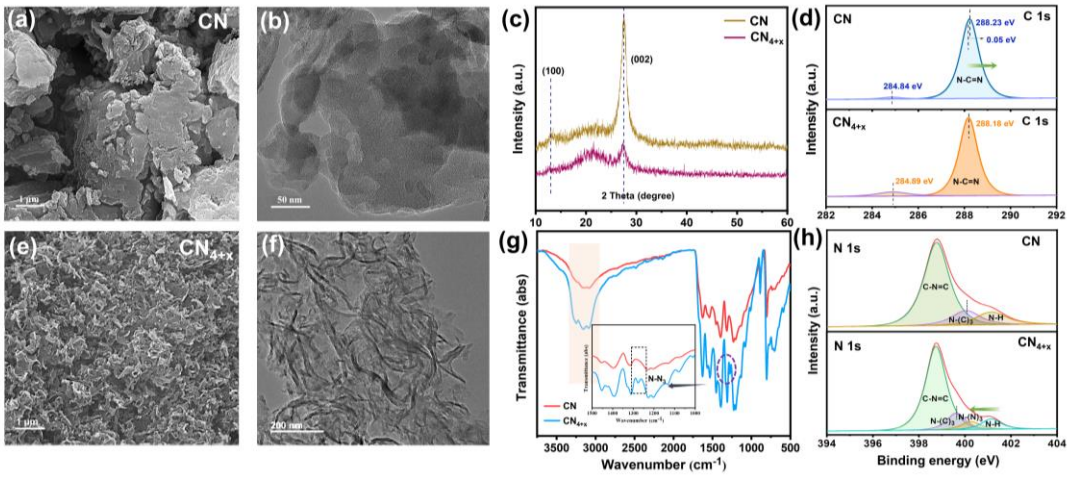

Fig. S9 (a)(e) SEM image for C_3N_{4+x} and bulk CN with different cooling times; (b)(f) TEM image for bulk CN and C_3N_{4+x}; (c) (g) XRD and FT-IR for bulk CN and C_3N_{4+x}; (d)(h) XPS spectra for bulk CN and C_3N_{4+x}

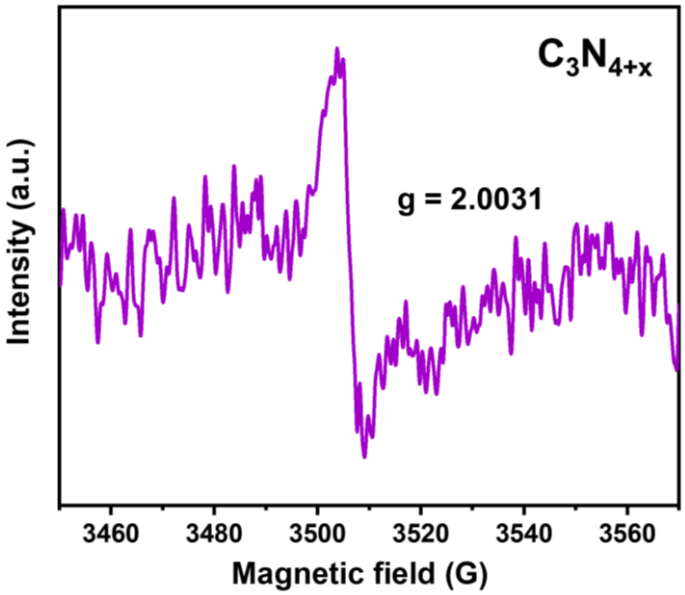

Fig. S10 EPR for C_3N_{4+x}

In addition, as we pointed out in our manuscript, the CN structure prepared contains a defect state structure, which we defined as nitrogen doping and therefore labeled as C_3N_{4+x}. The existence of this defect state may be due to the prolonged cooling and holding time during thermal polymerization.

References

[1] a) F. Weigend, R. Ahlrichs, *Physical Chemistry Chemical Physics* **2005**, *7*, 3297-3305; b) C. Adamo, V. Barone, *Journal of Chemical Physics* **1999**, *110*, 6158-6170.

[2] a) X. Cao, M. Dolg, H. Stoll, *The Journal of Chemical Physics* **2003**, *118*, 487-496; b) X. Cao, M. Dolg, *Journal of Molecular Structure: THEOCHEM* **2004**, *673*, 203-209; c) W. Küchle, M. Dolg, H. Stoll, H. Preuss, *The Journal of Chemical Physics* **1994**, *100*, 7535-7542.

[3] a) F. L. Hirshfeld, *Theoretica chimica acta* **1977**, *44*, 129-138; b) T. Lu, F. Chen, *Journal of Theoretical and Computational Chemistry* **2012**, *11*, 163-183; c) T. Lu, F. Chen, *Journal of Computational Chemistry* **2012**, *33*, 580-592.

[4] Z. Chen, J. Wang, M. Hao, Y. Xie, X. Liu, H. Yang, G. I. N. Waterhouse, X. Wang, S. Ma, *Nature Communications* **2023**, *14*, 1106.

[5] D. Zhao, Y. Wang, C.-L. Dong, Y.-C. Huang, J. Chen, F. Xue, S. Shen, L. Guo, *Nature Energy* **2021**, *6*, 388-397.

[6] a) R. Liu, Y. Chen, H. Yu, M. Položij, Y. Guo, T. C. Sum, T. Heine, D. Jiang, *Nature Catalysis* **2024**, *7*, 195-206; b) C. Shu, X. Yang, L. Liu, X. Hu, R. Sun, X. Yang, A. I. Cooper, B. Tan, X. Wang, *Angewandte Chemie International Edition* **2024**, *63*, e202403926; c) C. Chu, Z. Chen, D. Yao, X. Liu, M. Cai, S. Mao, *Angewandte Chemie International Edition* **2024**, *63*, e202317214; d) H. Yu, F. Zhang, Q. Chen, P.-K. Zhou, W. Xing, S. Wang, G. Zhang, Y. Jiang, X. Chen, *Angewandte Chemie International Edition* **2024**, *63*, e202402297; e) L. Cao, C. Wang, H. Wang, X. Xu, X. Tao, H. Tan, G. Zhu, *Angewandte Chemie International Edition* **2024**, *63*, e202402095; f) Y. Liu, L. Li, H. Tan, N. Ye, Y. Gu, S. Zhao, S. Zhang, M. Luo, S. Guo, *Journal of the American Chemical Society* **2023**, *145*, 19877-19884; g) C. Qin, X. Wu, L. Tang, X. Chen, M. Li, Y. Mou, B. Su, S. Wang, C. Feng, J. Liu, X. Yuan, Y. Zhao, H. Wang, *Nature Communications* **2023**, *14*, 5238; h) P. Ren, T. Zhang, N. Jain, H. Y. V. Ching, A. Jaworski, G. Barcaro, S. Monti, J. Silvestre-Albero, V. Celorrio, L. Chouhan, A. Rokicińska, E. Debroye, P. Kuśtrowski, S. Van Doorslaer, S. Van Aert, S. Bals, S. Das, *Journal of the American Chemical Society* **2023**, *145*, 16584-16596; i) T. Yang, D. Zhang, A. Kong, Y. Zou, L. Yuan, C. Liu, S. Luo, G. Wei, C. Yu, *Angew Chem Int Ed Engl* **2024**, *63*, e202404077; j) H. Cai, F. Chen, C. Hu, W. Ge, T. Li, X. Zhang, H. Huang, *Chinese Journal of Catalysis* **2024**, *57*, 123-132; k) Y. Zhang, Q. Cao, A. Meng, X. Wu, Y. Xiao, C. Su, Q. Zhang, *Advanced Materials* **2023**, *35*, 2306831; l) S. Wang, Z. Xie, D. Zhu, S. Fu, Y. Wu, H. Yu, C. Lu, P. Zhou, M. Bonn, H. I. Wang, Q. Liao, H. Xu, X.

Chen, C. Gu, *Nature Communications* **2023**, *14*, 6891; m) J. Zhang, H. Lei, Z. Li, F. Jiang, L. Chen, M. Hong, *Angewandte Chemie International Edition* **2024**, *63*, e202316998; n) C. Feng, J. Luo, C. Chen, S. Zuo, Y. Ren, Z.-P. Wu, M. Hu, S. Ould-Chikh, J. Ruiz-Martínez, Y. Han, H. Zhang, *Energy & Environmental Science* **2024**, *17*, 1520-1530; o) L. Li, X. Lv, Y. Xue, H. Shao, G. Zheng, Q. Han, *Angewandte Chemie International Edition* **2024**, *63*, e202320218.